

The Observational Basis For Central Engines in Gamma-Ray Bursts

E. E. Fenimore and E. Ramirez-Ruiz¹

MS D436, Los Alamos National Laboratory, Los Alamos, NM, 87545

Abstract.

We review the observational differences between gamma-ray bursts occurring on a single shell (such as in the external shock model) and multiple shells (such as in the internal shock model). The expected profile and average spectral evolution from a single shell is compared to the average of many bursts and found to be different. The presence of gaps in many gamma-ray bursts is a strong argument against a single shell because an observer should see many causally disconnected regions at any one time. The rapid variability is also difficult to explain from a single shell because of the large number of causally disconnected regions. The pulse width as a function of time in a burst should increase because there is a one-to-one relationship between arrival time and the off-axis angle of emission. The observations show that the pulse width does not increase with time. Finally, in GRB990123 there is evidence for deceleration from the simultaneous optical observations, yet the gamma-ray pulses show no lengthening of their pulse structure. We conclude that gamma-ray bursts are caused by a relatively small central engine.

1. Introduction

The rapid temporal evolution and GeV emission in gamma-ray bursts (GRBs) indicate relativistic motion with bulk Lorentz factors of at least 100. Two competing explanations have been suggested to explain the rapid time variability. In the “external” shock model (Mészáros & Rees 1993) there is a very quick (< 1 s) release of energy at a central site that produces an expanding relativistic shell. That shell interacts over a long period of time ($10^6 - 10^7$ s) with the interstellar medium (ISM), producing multiple releases of gamma rays. The shell keeps up with the photons it produces in such a way that they are separated (spatially) by a few light-seconds even though they were emitted over a long period of time. These bursts of gamma rays arrive at the detector over a modest range of times (10 - 100 s).

The alternate theory is that the release of energy at the central site is sporadic and lasts as long as we observe the burst to last. Each release forms

¹Also Facultad de Ciencias, Universidad Nacional Autónoma de México, Distrito Federal, México 04510

a shell which is closely related to an observed peak. The gamma rays might result from shocks that occur when one shell runs into another and, hence, these models are often called “internal” shocks (Rees & Mészáros 1994).

In this review, we present analyses based on causality and kinematics that strongly argue that the GRB phase occurs in a small region and not on a single shell. We will establish six scenarios that cover all kinematically allowed ways for a single shell to produce the gamma-ray time history. Observational evidence will rule out all six. We conclude the source must be smaller, as in the internal shock model. We do not argue against external shocks or for internal shocks, *per se*, but rather against a single shell and for a central engine that is small enough to produce the typical GRB time history without violating causality or other kinematic limits.

Given the large Lorentz factor, Γ , of the shell, one only sees photons from the portion of the shell that is within angles $\sim \pm\Gamma^{-1}$ about the line of sight. Thus, the shell must effectively be aimed directly at the observer. In such a situation, the temporal variations in an observer’s detector do *not* tell the observer what time scale the source varied in the *observer rest frame*. Time in a detector is not the detector’s rest frame time. Rest frame time must be measured by clocks placed at all sites in the rest frame. Rather, a detector measures when the photons arrive at a single location. Normally this distinction plays no role, but it does when the source is moving towards the observer. This is not due to Lorentz transformations but due to superluminal effects. Consider a photon which is emitted by the shell as the shell leaves the central site. If another photon is emitted t sec later, it is behind the first photon by only $(c - v)t = ct/(2\Gamma^2)$ where v is the velocity of the shell, $\beta = v/c$, and $\Gamma = (1 - \beta^2)^{-1/2}$. These two photons will arrive at the detector separated in time by $T = t/(2\Gamma^2)$. (We denote the detector’s rest frame time with t and the arrival time with T .) In contrast, clocks moving with the shell would measure time t' which is related to the observer’s rest frame time by the Lorentz factor: $t = \Gamma t'$. So, if a shell expands in the detector rest frame for 10^7 s and $\Gamma = 200$, the detector sees photons for 125 s while a clock on the shell would see emission for 25,000 s.

Most results in this paper originate from the observation that the average profile of GRBs tend to have a fast rise and slower decay. The relatively fast rise (<20% of the duration) says that the shell is active only over a short period. As a result, the profile is dominated by curvature and there is a one-to-one relationship between the originating angle of the emission and the time of arrival at the detector.

The curvature of the shell is actually more important than the expansion. The curvature is extremely small, but the expansion is contracted by $2\Gamma^2$. Photons produced from a part of the shell that is at an angle θ off the line of sight to the observer must travel an additional distance: $ct(1 - \cos\theta)$. For an angle near $\theta = \Gamma^{-1}$, this additional distance corresponds to a delay in arrival time of $t/(2\Gamma^2)$, the same as the separation in time due to the expansion.

The six possible emission geometries from a single shell are shown in Figure 1. For example, the first (Fig. 1a) is the classic single shell that coasts for a while and then turns on. Figure 1 will be explained as we discuss various observations.

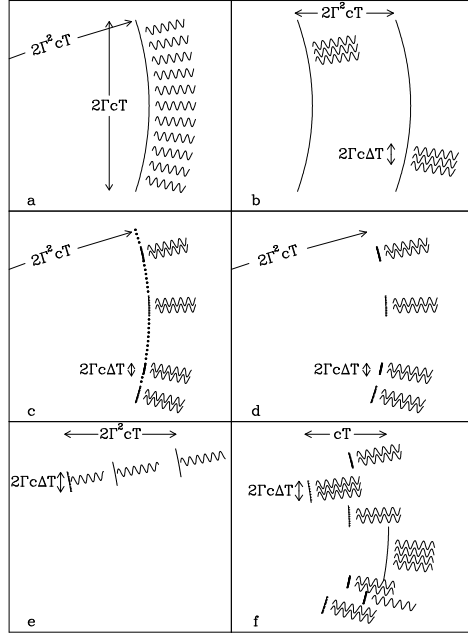


Figure 1. Possible emission geometries for a single relativistic shell. The observed average profile of GRBs has a sharp rise and slow decay which is inconsistent with scenarios with full shells that emit over a wide range of radii (b, f). Gaps in GRBs are inconsistent with scenarios that have full shells and emit over a short range of radii (a, c, d). The observed low filling factor indicates that most of the angular size available to the shell does not emit. This implies that the energy reservoir for the burst must be ~ 1000 times larger than estimated from the observed gamma-ray flux if the non-emitting regions (denoted by dots in c) have bulk energy as do the regions that emit. If the burst consists of many fine jets, the reservoir does not have to be larger (see d). Scenario (e) uses a narrow jet to get rid of curvature effects so it can more easily have gaps and the average profile. However, to have constant pulse width throughout the burst, it requires no deceleration. GRB990123 shows deceleration during the burst, arguing against scenario (e).

2. Expected Emission from a Single Shell

Assume the shell expands for a time (t_e) in a photon quiet phase and then emits uniformly for a short period of time (i.e., scenario [a] in Fig. 1). That is, the production of photons is $P(t) = P_0\delta(t-t_e)$. In terms of arrival time, the *on-axis* emission will arrive at $T_e = t_e/(2\Gamma^2)$ and the off-axis emission will arrive later. The relationship between the angle on the shell and the arrival time depends only on the time since the shell left the central site (if Γ is constant, Fenimore, Madras, & Nayakshin 1996):

$$2\Gamma^2(1 - \beta \cos \theta) = (T/T_e) . \quad (1)$$

This equation establishes a one-to-one relationship between the angle at which photons originate and the time at which they *arrive* at the detector. It is from this equation that we determine how the observed time history should evolve. The observed temporal variability (V) is found by integrating over the volume where photons arrive at the detector at the same time and including relativistic beaming. For the δ -function production of photons in time (and radius), the expected shape is (Fenimore, et al. 1996):

$$\begin{aligned} V_\delta(T, T_e) &= 0 && \text{if } T < T_e , \\ &= \psi T_e \left(\frac{T}{T_e} \right)^{-\alpha-1} && \text{if } T > T_e \end{aligned} \quad (2)$$

where we have assumed that the rest frame photon-number spectrum is isotropic with a power law with index $-\alpha$, and ψ is a constant. This envelope is similar to a “FRED” (fast rise, exponential decay) where the shape of the slow, power law decay depends only on the time that the shell expands before it emits (T_e). The decay phase is due to photons delayed by the curvature. If GRBs had this shape, we could determine a best-fit T_e . As a rule of thumb, $T_e \sim 5T_{FWHM}$ where T_{FWHM} is the full width at half maximum of the profile (Fenimore et al. 1996).

The expected spectral variation can also be found. GRB spectra can often be fit by the so-called “Band” model (Band et al. 1993) which consists of two power laws and the peak of the νF_ν distribution. If E'_p is the peak of νF_ν in the rest frame of the shell, the observed E_p is Doppler boosted. The delayed photons are boosted less because they originate from regions moving at the angle θ relative to the on-axis regions. The Doppler boost as a function of arrival time is

$$B_\delta(T, T_e) = [\Gamma(1 - \beta \cos \theta)]^{-1} = \frac{1}{2\Gamma} \left(\frac{T}{T_e} \right)^{-1} . \quad (3)$$

This equation establishes a one-to-one relationship between Doppler boost and the time at which they *arrive* at the detector (Fenimore et al. 1996).

More complex envelopes can be found from weighted sums of $V_\delta(T, T_e)$. For example, the shell might emit for a range of times during which it collides with something. We model $P(T_e, T_0)$ to be non-zero from t_0 to t_{\max} , and we assume $P(T_e, T_0)$ can be approximated as a power law:

$$P(T_e, T_0) = P_0(T_e/T_0)^{-\eta} . \quad (4)$$

In terms of arrival time, the *on-axis* emission will arrive between $T_0 = t_0/(2\Gamma^2)$ and $T_{\max} = t_{\max}/(2\Gamma^2)$. The expected envelope, $V(T)$, is:

$$V(T) = \int_{T_0}^T V_{\delta}(T, T_e) P(T_e, T_0) dT_e . \quad (5)$$

Due to the curvature of the shell, off-axis photons will be delayed, and most emission will arrive later:

$$\begin{aligned} V(T) &= 0 && \text{if } T < T_0 \\ &= \frac{\psi P_0}{\omega T_0^{-\eta}} \frac{T^{\omega} - T_0^{\omega}}{T^{\alpha+1}} && \text{if } T_0 < T < T_{\max} \\ &= \frac{\psi P_0}{\omega T_0^{-\eta}} \frac{T_{\max}^{\omega} - T_0^{\omega}}{T^{\alpha+1}} && \text{if } T > T_{\max} \end{aligned} \quad (6)$$

where $\omega = \alpha + 3 - \eta$ (Fenimore et al. 1996).

The envelope in equation (6) is similar to equation (2), that is, a ‘‘FRED’’ where the rise depends mostly on the duration of the photon active phase ($T_{\max} - T_0$) and the slow, power law decay depends mostly on the final overall size of the shell (T_{\max}).

3. Average Profile and Spectral Evolution

The predicted profile of GRBs (Eq. [6]) and spectral evolution (Eq. [3]) can be compared to the average profile and average spectral evolution of GRBs (Fenimore 1999). The average profile can be found by scaling the duration of each burst by a constant before they are averaged. This can be viewed as an ‘‘aligned $T_{\langle \text{Dur} \rangle}$ ’’ average in contrast to the ‘‘aligned peak’’ averages, such as those used by Mitrofanov, Litvak, & Ushakov (1997). In the aligned peak average, each burst contributes to the average by aligning the largest peak. The time scale of the peak is conserved as it contributes to the average. In the aligned $T_{\langle \text{Dur} \rangle}$ average, each burst contributes to the average by aligning the midpoint of the burst, and the time scale of the burst is adjusted to a standard duration which we call $T_{\langle \text{Dur} \rangle}$.

The Burst and Transient Source Experiment (BATSE) catalog provides durations called T_{90} and T_{50} (Meegan et al. 1996). For example, T_{90} is the duration which contains 90% of the counts. It is defined by finding the duration that excludes the first 5% and last 5% of the counts in the burst. There is a similar definition for T_{50} . We estimate an average duration, $T_{\langle \text{Dur} \rangle}$, from T_{90} and T_{50} . To first order, $T_{\langle \text{Dur} \rangle}$ is $T_{90}/0.9$ or $T_{50}/0.5$. By definition, the beginning point for T_{90} or T_{50} must be at a point at which the count rate is increasing. Thus, if we stretched each burst to a standard duration by scaling the time by some multiple of T_{90} , there would be a coherent peak at the first 5% point and at the last 5% point. Rather, we define $T_{\langle \text{Dur} \rangle}$ to be a combination of T_{90} and T_{50} to break up the coherency. Specifically, we define

$$T_{\langle \text{Dur} \rangle} = \frac{(T_{90} + T_{50})/2}{0.7} . \quad (7)$$

In Figure 2 we used the BATSE CONT data to investigate the average spectral

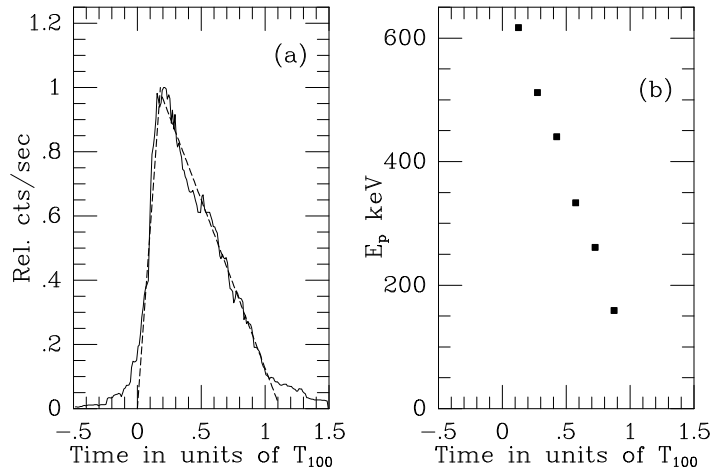


Figure 2. The average temporal and spectral evolution of bright events with intermediate durations (T_{90} between 16 and 40 sec). (a) The average time history. The decay phase starting 20% after the beginning of the $T_{\langle \text{Dur} \rangle}$ period is inconsistent with exponential decays and power law decays. Instead, the decay is consistent with a linear slope. (b) The average spectral evolution. The spectral evolution is found by fixing the low energy and high energy slopes at the average for the bursts and allowing only the peak of the νF_ν distribution to vary. The peak energy is also a linear function. Thus, on average, the intensity is a linear function of the peak of the νF_ν distribution. This temporal and spectral evolution is inconsistent with that expected from a single shell. From Fenimore (1999).

and temporal evolution. The BATSE CONT data has 16 energy channels and 2.048 s time resolution. We used the 32 BATSE 3B events with T_{90} between 16 and 40 s since those events have a sufficient number of CONT samples to investigate the spectral evolution.. The resulting average time history appears to rise to a peak and then fall linearly. We have fit a variety of temporal shapes to the decay portion between 20% after the beginning of the $T_{\langle \text{Dur} \rangle}$ period to the end of the $T_{\langle \text{Dur} \rangle}$ period. We fit a linear function, an exponential function, and power law decays. We particularly checked if a $T^{-1.4}$ power law would fit because that type of decay is seen later during the x-ray afterglows (Piro, Matt, & Ricci 1997). The linear fit was the best fit (Fenimore 1999). The power law and exponential fit had χ^2 values that were 2.2 and 3.8, respectively, times larger and they disagreed with the observations in a systematic way, failing to agree with the observations at the ends of the time range. A power law with an index of -1.4 had a χ^2 that was 6.4 times larger than the linear fit. The best linear function is:

$$\begin{aligned}
 I &= 5.56 \frac{T}{T_{\langle \text{Dur} \rangle}} && \text{if } T < 0.18 T_{\langle \text{Dur} \rangle} \\
 &= 1.19 - 1.06 \frac{T}{T_{\langle \text{Dur} \rangle}} && \text{if } T > 0.18 T_{\langle \text{Dur} \rangle} .
 \end{aligned}
 \tag{8}$$

We calculated aligned $T_{\langle\text{Dur}\rangle}$ averages for each of the 16 CONT energy channels. From these, six spectra were formed, each covering 15% of the $T_{\langle\text{Dur}\rangle}$ range. The first one started 5% after the beginning of the $T_{\langle\text{Dur}\rangle}$ range, and the last one ended at 5% before the end of the $T_{\langle\text{Dur}\rangle}$ range. For each of these spectra, we fit the “Band” spectral shape (Band et al., 1993). This shape consists of a low energy slope (α), the peak of the νF_ν distribution (E_p), and a high energy slope (β). We first fit the Band shape to the sum of all six spectra. To investigate the average spectral evolution, we analyzed each of the six spectra separately, fixing α and β to their average value. Thus, the only free parameter is E_p . Figure 2b shows the resulting spectral evolution. It is a remarkably straight line:

$$E_p = 680 - 600 \frac{T}{T_{\langle\text{Dur}\rangle}} \quad \text{keV} \quad . \quad (9)$$

The decay phase of the average GRB profile argues against scenarios that generate photons from a small range of radii (i. e., a, c, d in Fig. 1). The expected profile from a small range of radii should have a power law decay phase (i.e., $T^{-\alpha-1}$, where $\alpha \sim 1.5$) and the peak of νF_ν should evolve as T^{-1} (see eqs. [3,6]). The observations indicate linear decays.

The rise phase of the average GRB profile argues against scenarios that generate photons over a large range of radii (i. e., b, f). For example, in scenario (b), a small portion of the shell emits at one radius (small portion to produce the observed small ΔT 's) and then moves to another radius where another small portion emits. The shell has such activity for a long time, $t_{\text{max}} - t_0$, but the shell keeps up with the photons it produces. The resulting duration in arrival time is $T_{\text{max}} - T_0 = (t_{\text{max}} - t_0)/(2\Gamma^2)$. The average profile should reflect the increasing surface area as the shell moves, that is, equation (6) gives a long rise and short decay rather than the observed short rise and long decay.

In fact, expansion should not eliminate curvature effects, even in the extreme case of $T_0 = 0$ in equation (6). Dermer & Mitman (1999) have modeled gamma-ray generation by small clouds spread out over a wide range of radii, effectively scenario (b). Their profiles tend to have longer rises than observed because $T_{\text{max}} - T_0$ in equation (6) is large. The pulses at the end of their bursts are noticeably longer due to residue curvature effects (and deceleration). If they had restricted their clouds to a smaller range of radii, the profile would have a faster rise, but then the curvature effects would be stronger.

Scenario (f) also emits over a range of radii although much shorter than scenario (b). Scenario (b) emits at different radii *and* different times. The shell keeps up with the photons it produces so the range of time is contracted by $2\Gamma^2$. In scenario (f), the shell is fragmented, so exists at different radii at the same time. The fragments can emit at different radii but at nearly the same time. The photons are born with the separation that produces the observed duration. So, the range of radii in scenario (f) is cT , much shorter than in scenario (b). The fragments in scenario (f) appear to be independent of each other and there is no clear reason why the resulting average profile would have a short rise or long decay.

4. Filling Factor

The rapid variability seen in GRBs implies small spatial structures. The few number of peaks in GRBs implies only a few such structures. Thus, only a fraction of the surface of the shell becomes active. We define the “surface filling factor” to be that fraction. (Fenimore et al. 1996, 1999b). Let A_N be the area of an entity and N_N be the number of entities that (randomly) become active during the interval T_{obs} . If A_{obs} is the area of the shell that can contribute during T_{obs} , then the surface filling factor is

$$f = N_N \frac{A_N}{A_{\text{obs}}} = N_N \frac{A_N}{\eta A_S} \quad (10)$$

where η is the fraction of the visible area of the shell (A_S) that contributes during the interval T_{obs} .

The number of entities can be determined from the observed fluctuations in the time history. Variations about the overall envelope are due to a combination of the Poisson variations in the number of emitting entities and the Poisson variations associated with the count statistics. Assume for the moment that the contribution due to the count statistics are small such that the variations come from the Poisson variations in the number of contributing entities. We first remove the envelope by fitting a polynomial function to it. The observations are divided by the polynomial function, so the result is a flat envelope with variations due to the number of entities that, on average, are active simultaneously. The rate of occurrence of the entities, μ_N , can be found directly from the variations because the observed mean level is $K\mu_N$ where K is some constant and the variance is $K^2\mu_N$. We define N to be the observed mean level of the flattened envelope and δN to be the root mean square of the flattened envelope. In the case of no contribution from the counting statistics, μ_N would be $(N/\delta N)^2$. Here, we have implicitly assumed that all entities are identical. This is supported by the fact that peaks within GRBs usually are similar to each other. The actual root mean square of the flattened envelope is a combination of the variance due to the entities and the variance due to the counting statistics, σ_{CS}^2 . We assume they add in quadrature, that is, $N^2/(\delta N)^2 = \mu_N + \sigma_{CS}^2$. We estimate σ_{CS} to be root mean square of many Monte Carlo realizations of the flattened envelope. The rate of occurrence of entities is

$$\mu_N = \frac{N^2}{(\delta N)^2} - \sigma_{CS}^2 \quad (11)$$

This rate is the number of events per the time scale of the entities. Thus, the total number of entities that occur within a period T_{obs} is

$$N_N = \mu_N \frac{T_{\text{obs}}}{\Delta T_p} \quad (12)$$

where ΔT_p is the time scale for a single entity.

We have consider several processes that relate the size of an entity causing a peak to an observed peak duration, ΔT_p . Here, we consider the two most likely processes for the formation of a peak: regions that grow and regions formed by the interaction with the ISM.

Consider a gamma-ray producing region that grows at a speed near that of light, c_s , for a period $\Delta t'$ in the rest frame of the shell where presumably the region is symmetric. This growth might be associated with a developing shock. Let $\Delta r'_{\parallel}$ be the radius of the region in the rest frame along the direction of the motion and $\Delta r'_{\perp}$ be the radius in the perpendicular direction such that

$$\Delta r'_{\parallel} = \Delta r'_{\perp} = c_s \Delta t' = c_s \Gamma^{-1} \Delta t \quad . \quad (13)$$

The sizes in the rest frame of the detector are related to the sizes in the rest frame of the shell as: $\Delta r_{\parallel} = \Gamma^{-1} \Delta r'_{\parallel}$ and $\Delta r_{\perp} = \Delta r'_{\perp}$.

Combining the effects of the movement of the shell during the growth with the maximum size that the entity can grow in time Δt , we find that the duration in arrival time is

$$\Delta T_p = \frac{\Delta t}{\Gamma^2} \left[\left(\frac{1}{2} \right)^2 + \left(\frac{c_s}{c} \right)^2 \right]^{1/2} \quad . \quad (14)$$

The size of the emitting entity is

$$A_N = \pi \Delta r_{\perp}^2 = \pi \left(\frac{c_s \Delta t}{\Gamma} \right)^2 = \frac{\pi c_s^2 \Gamma^2 \Delta T_p^2}{\left[\left(\frac{1}{2} \right)^2 + \left(\frac{c_s}{c} \right)^2 \right]} \quad . \quad (15)$$

The alternative cause of a peak resulting from the shell is that the shell interacts with an ambient object such as an ISM cloud. Presumably, the object is symmetric such that $\Delta R_{\perp} = \Delta R_{\parallel} = \Delta R_{\text{amb}}$. (We use lower case Δr for an object that grows in a shell and upper case ΔR for an ambient object.) The contribution to the peak duration from the time the shell takes to move through the cloud (i.e., $\Delta R_{\text{amb}}/[c\Gamma^2]$) is negligible compared to the time the shell takes to engage the perpendicular size of the object. This engagement time is caused by the curvature of the shell. At an angle θ from the line of sight, the time to engage the object is $\Delta T_{\Delta R_{\perp}} = \theta \Delta R_{\text{amb}}/(2c)$. Note that Table 2 of Fenimore et al. (1996) was incorrect for $\Delta T_{\Delta R_{\perp}}$; see Sari & Piran (1997). At a typical angle of $\theta \sim \Gamma^{-1}$,

$$\Delta R_{\text{amb}} = \frac{c \Delta T_p \Gamma}{2} \quad (16)$$

and

$$A_N = \pi \Delta R_{\text{amb}}^2 = \frac{\pi c^2 \Gamma^2 \Delta T_p^2}{4} \quad . \quad (17)$$

Thus, both the case of shocks that grow from a seed and the case of shells running into ambient objects are similar. If $c_s = c/3$, then A_N from equation (15) is 16/13 times larger than from equation (17). These two scenarios only differ by a constant the order of unity.

A common misconception is that one can just use an ISM cloud that covers most of the shell's surface. Only the instantaneous interaction between two *plain parallel* surfaces oriented perpendicularly to our line of sight can produce a short peak from large surfaces. A curved surface has sources limited in size to that of equation (17).

The final ingredient for the calculation of the surface filling factor is the area of the shell visible to the observer:

$$A_S = 2\pi R^2(T)(1 - \cos \theta_{\text{max}}) \quad , \quad (18)$$

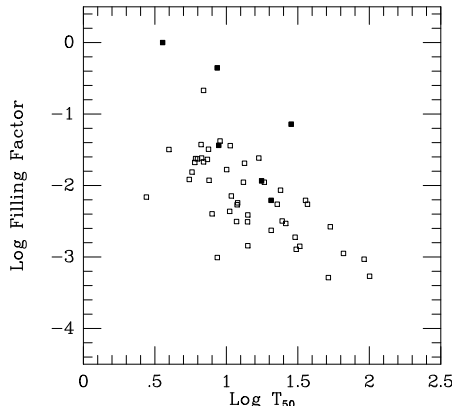


Figure 3. Typical values of the fraction of a relativistic shell that becomes active during a GRB as a function of the duration of the emission (T_{50}). The six solid squares are FRED-like BATSE bursts for which direct estimates of the size of the shell can be made. The 46 open squares are long complex BATSE bursts where we estimate the size in a manner similar to the FRED-like estimate. Under most conditions, the efficiency is $\sim 0.1\Delta T/T$. These low values imply that either only a small fraction of the shell converts its energy into gamma-rays or that GRBs consist of very fine jets with angular sizes much smaller than Γ^{-1} . From Fenimore et al. (1999b).

where θ_{\max} is either the angular width of the shell or it is $\sim \Gamma^{-1}$, whichever is smaller. Before the shell starts to decelerate, presumably θ_{\max} is larger than Γ_0^{-1} . Using $R(T) = 2\Gamma_0^2 cT$,

$$A_S = \pi[\Gamma_0^{-1}R(t)]^2 = 4\pi c^2\Gamma_0^2 T^2 \quad . \quad (19)$$

Thus, during the constant Γ phase, the filling factor is

$$f = N_N \left[\frac{\Delta T_p}{T} \right]^2 \frac{1}{k\eta} = \left[\frac{N^2}{(\delta N)^2} - \sigma_{CS}^2 \right] \frac{\Delta T_p}{k\eta T} \quad (20)$$

where k is 16 for ambient objects and 13 for entities that grow from a seed (see differences between equations (15) and (17)).

From the expected envelope (eq. 6), η is 1 when $T = 0.8T_{50}$ (Fenimore et al. 1999b). Thus, the filling factor can be found from T_{50} , the mean and variance of the GRB time history, Monte Carlo estimates of σ_{CS}^2 , and the typical widths of individual pulses such as found by Norris et al. (1996). In Figure 3 we show the distribution of surface filling factors as a function of burst duration T_{50} . The solid squares are the FRED-like bursts, and the open squares are the long complex bursts. Although some of the smooth FRED-like bursts can have surface filling factors near unity, most bursts have values on the order of 5×10^{-3} .

Small filling factor implies two things. First, that one should see many peaks in GRBs, the order of $(T/\Delta T)^2 \sim 10^4$. Second, if the filling factor is small because there are many more places on the shell that do not convert their

bulk energy to gamma rays, then the energy reservoir needs to be f^{-1} times larger (Fenimore et al. 1996, Sari & Piran 1997).

Consider scenarios (c) and (d) in Figure 1. In both, only a single radius becomes active, as consistent with the observed fast rise of the average GRB profile. In both, only a fraction of the surface becomes gamma-ray active. In scenario (c), only patches on the shell become active so the inter-patch regions (denoted by the dotted lines in Fig. 1c) do not convert their kinetic energy to gamma-rays. Scenario (d) is very similar except the inter-patch regions are devoid of material. Effectively, scenario (d) is many narrow jets. Small filling factor raises the required energy reservoir only in scenario (c) but not (d). We estimate the energy requirement by observing the gamma-ray flux at earth and making corrections (i) for the distance to the object, (ii) for emission not seen because it beamed away from us, and (iii) for the efficiency of converting bulk energy into gamma-rays. Corrections (i) and (ii) are the same for all scenarios. Correction (iii) will always include correcting for the microscopic physics of generating gamma rays. Small filling factor implies a macroscopic issue: are there portions of the shell that never (or barely) converts its bulk energy? Most of the bulk energy in scenario (c) is never converted to gamma rays so it requires a reservoir that is f^{-1} time larger than for scenario (d).

In other scenarios (e. g., b, f), the low filling factor also implies a few emitting entities relative to the available surface area. If that is accomplished by having the rest of the surface area not convert its energy, the energy requirement will be larger by f^{-1} . If it is accomplished by many fine jets, the energy reservoir needs not be larger.

We consider it unlikely that most of the shell never produces gamma-rays, especially if the process involves forming an external shock in the ISM. The ISM should decelerate all portions of a shell. However, the alternative (many fine jets in scenario [d]) is unlikely from hydrodynamic considerations (Sari & Piran 1997). When the opening angle of a jet is less than Γ^{-1} , the jet will expand preventing such fine jets. Thus, a low filling factor (with or without requiring a larger energy reservoir) presents a strong case against scenarios b, c, d, and f.

5. Gaps

Gaps or precursors in GRBs produce one of the strongest arguments against a single relativistic shell. The sharp rise in the average profile (see section 3) indicates that the shell emits for a short period of time (i.e., t_0 to t_{\max} in eq. [6] is short relative to the duration of the event), so that the shape of the overall envelope is dominated by photons delayed by the curvature. During the decay phase, the one-to-one relationship between time of arrival and angle (eq. [1]) means that, at any one time, only an annulus oriented about the line of sight contributes photons to the observer. Gaps in the time history indicate that some annuli emit while others do not (see Fig. 4). From equation (15) we know that the maximum radius of a causally connected region is $2c\Gamma\Delta T$ whereas the radius of the visible shell is $2c\Gamma T$ (cf. eq. 19). Thus, for gaps to occur, a large, causally disconnected annulus about the line of sight must coordinate its emission. This is the strongest argument against scenarios consistent with the rapid rise of the

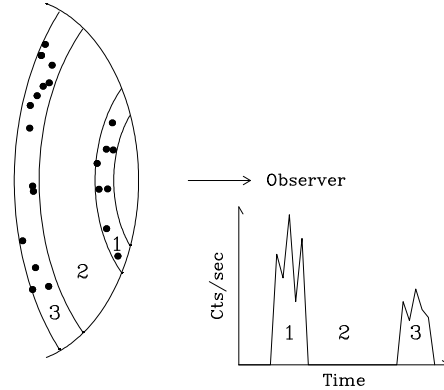


Figure 4. Schematic of the relationship between the emission on a shell and the observed time history. The curvature delays the photons from off-axis regions such that at any one time, the observer sees photons from an annulus oriented around the line of sight. The perpendicular size of the shell is $\sim 2c\Gamma T$ whereas a causally connected entity (represented by the dots) is only $2c\Gamma\Delta T$. Here, T and ΔT are the time in the time history and a typical time scale of variation. Gaps imply that large causally disconnected regions do not emit (e.g., region 2 produces gap 2 in the time history). The number of entities in each annulus determines the variability of the time history. The “filling factor” is the fraction of the shell occupied by the emitting entities and is typically 10^{-3} .

average profile, that is, those that use a full shell emitting over a short range of radii (scenarios a, c, d in Fig. 1).

6. Constant Pulse Width

A visual inspection of the BATSE catalog of multiple-peaked time histories reveals that peaks usually have about the same duration at the beginning of the burst as near the end of the burst. The aligned peak method measures the average pulse temporal structure, each burst contributes to the average by aligning the largest peak (Mitrofanov 1997). To characterize the average evolution of peak widths with time, we used all 53 bursts from the BATSE 4B Catalog that were longer than 20s and brighter than $5 \text{ photons s}^{-1} \text{ cm}^{-2}$. Each burst was required to have at least one peak, as determined by a peak-finding algorithm (similar to Li & Fenimore 1996), in each third of its duration. The largest peak in each third was normalized to unity and shifted in time, bringing the largest peaks of all bursts into common alignment. This method was applied in each third of the duration of the bursts. Thus, we obtained one curve of the averaged pulse shape for each third of the bursts (as shown in Figure 5). The average profile is notably identical in each $1/3$ of T_{90} , the difference in widths is less than 1%.

There are two sources of pulse width from a shell: angular effects and deceleration. Assuming that the pulse duration in the rest frame of the shell is

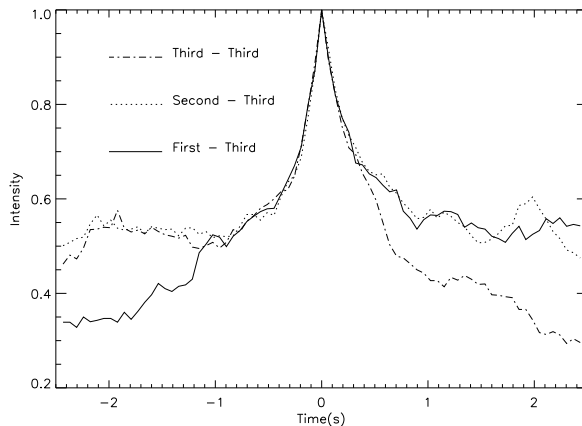


Figure 5. Average peak alignment from 53 bright BATSE bursts with durations longer than 20 s. The three curves show the average pulse shape for the largest peak in the first third, second third, and last third of the bursts. We find no significant change, during the gamma-ray phase, in the average peak width over at least $2/3$ of T_{90} . From Ramirez-Ruiz & Fenimore (1999).

not dependent on the direction to the observer, the pulse width at two times A and B are related as

$$\frac{\Delta T_B}{\Delta T_A} = \frac{\Gamma_B(1 - \beta \cos \theta_B)}{\Gamma_A(1 - \beta \cos \theta_A)} \quad (21)$$

where θ_B and θ_A are the angles responsible for the emission. From equation (1),

$$\Gamma(1 - \beta \cos \theta_A) = \frac{T_A}{2\Gamma T_0} \quad (22)$$

where T must be measured from when the shell left the central site and T_0 is the time of the peak of the emission. Before the shell decelerates, $\Gamma(T)$ is constant and pulse widths ought to scale at T_B/T_A . Thus, the lack of pulse width evolution in Figure 5 is strong evidence against scenarios (c) and (d) where there is a strong relationship between angle and time.

Scenario (f) attempts to get around the constant peak width constraint by upsetting the one-to-one relationship between arrival time and angle. If Γ varies on an angular scale much smaller than Γ^{-1} , the shell could fragment. After coasting for a while, the fragments would be spread out in time commensurate with the observed duration of GRBs. This requires variations in Γ of at least a factor of $\sqrt{2}$ (Fenimore, et al. 1996, 1999b). The peaks arrive at the detector arranged by the value of Γ of the fragment that produce the emission. Although we cannot specify what process actually makes the peaks, it is surprising that the resulting peaks have very consistent pulse width yet were formed from a systematic trend in Γ .

The only way to be consistent with gaps, low filling factor, short rise time in the average profile, and constant peak width is scenario (e), that is, a very

narrow jet (to eliminate curvature effects and allow a low filling factor) with no deceleration (to be consistent with constant pulse width).

7. GRB990123

On January 23, 1999, the Robotic Optical Transient Search Experiment (ROTSE) discovered strong optical emission (9th mag) during a gamma-ray burst (Akerlof et al. 1999). This behavior was predicted a few weeks before (Sari & Piran 1999a). The optical emission peaked at about 45 s after the trigger and is very consistent with the emission expected from forward and reverse external shocks that form when the shell decelerates in the ISM (Sari & Piran 1999b). This provides an excellent opportunity to test scenario (e) in Figure 1. Scenario (e) is consistent with constant pulse widths, gaps, the average profile, and small filling factor *if* the shell is not decelerating. Since there is gamma-ray emission after the optical peak in GRB990123, we can test it for a widening of the pulses. If the gamma-ray are being made on the single shell responsible for the optical emission, we ought to see the pulses widen due to the deceleration.

After deceleration started, during the afterglow, $\Gamma(T) \propto T^{-3/8}$ so the combined effects of angle and deceleration at a typical angle of $\theta = \Gamma^{-1}$ gives from equation (21):

$$\frac{\Delta T_B}{\Delta T_A} = \left[\frac{T_B}{T_A} \right]^{11/8}. \quad (23)$$

If the shell is relatively narrow (range of $\theta < \Gamma^{-1}$) as in scenario (e), then the pulses only grow due to the deceleration:

$$\frac{\Delta T_B}{\Delta T_A} = \left[\frac{T_B}{T_A} \right]^{3/8}. \quad (24)$$

We analyzed four periods after the peak of the optical emission in a manner similar to Figure 5 (Fenimore, Ramirez-Ruiz, Wu 1999a). It is likely that the shell started to leave the central site at about the time when the first gamma rays were emitted. BATSE detected emission quite early in this burst, so we will use the BATSE time for T . The first time we analyzed is at ~ 45 s after the start and last time is at ~ 82 s. Based on this, we expect the pulse widths to increase by about a factor of 2.3 (eq. [23]) if the shell is wider than Γ^{-1} , and 1.25 (eq. [24]) if the shell is much narrower than Γ^{-1} . We found that $\Delta T_B/\Delta T_A$ was 1.034 ± 0.035 . The minimum expected from just deceleration was rejected at the 6σ level. Thus, we conclude that scenario (e) can be rejected as well: the pulses do not get wider when the shell is decelerating.

8. Summary

GRBs time histories display two salient features: long durations and chaotic variations. We have presented six scenarios for how a single relativistic shell produces these features. These scenarios differ primarily in how they explain *duration*. Some produce the long duration by delays caused by the curvature of the shell (a, c, d in Fig. 1). Curvature dominates when the shell emits effectively

at one radius and one time. Scenarios (a, c, d) differ in how they produce the chaotic variations. Duration associated with expansion (scenarios b, e) are caused by a shell that emits at different radii and different times. Scenario (b) still has some curvature effects while (e) emits over a very narrow angle. The scenario (f) shell has lost its curvature due to different parts of the shell having different speeds. The parts spread out and emit at about the same time, but at radii that are separated by distances that light can travel during a typical GRB duration.

A shell that coasts and then emits over a very short range of radii (and therefore, time) will have a duration set by the curvature. Indeed, the average GRB profile has a sharp rise and long decay characteristic of a profile made by curvature. However, the details of the decay do not match the observations, the decay is linear whereas power laws were expected. That difference is probably not large enough to reject curvature as the source for the duration. Gaps provide the most potent argument against models that rely on curvature. Gaps indicate that some large causally disconnected regions in an annulus about the observer’s line of sight emit while others do not. This point alone should eliminate scenarios (a, c, d).

The second problem with curvature is that the one-to-one relationship of arrival time with angle on the shell implies that pulses should get wider later in the burst because the Lorentz factor changes. This is not observed.

Scenario (b) uses expansion to produce the duration. Expansion has a phase when the available surface area (i. e., within Γ^{-1}) grows with time and, therefore, the expected average profile should have a long rise ($T_{\max} \gg T_0$ in eq. 6). The observed fast rise in the average profile eliminates this scenario. In addition, even in an extreme case ($T_0 = 0$), the curvature effects are comparable to the expansion effects. One should still see some increase in the pulse width during the burst and none is seen. Scenario (e) avoids both problems by being very narrow: no increase in surface area and no curvature to contend with. To be consistent with constant pulse width would require no deceleration, but that is what is observed in GRB990123.

Scenario (f) avoids curvature effects by breaking up the shell and avoids expansion effects by using spatial distances to get the burst duration. There is no apparent reason why it would produce the average burst profile.

The large number of causally disconnected regions while we see relatively few peaks in GRBs leads to low “filling factor”. Only about 10^{-3} of the available surface becomes active. This is a strong argument against scenarios (c) where the non-emitting regions of the shell have bulk energy that is never converted to gamma-rays. Scenario (d) eliminates those regions by being many fine jets. Scenarios (b, f) would also either require much more energy or be made up of many fine jets to accommodate the low filling factor.

Our scenarios span the combinations of emission at constant radii, constant time, varying radii, and varying time except one: roughly constant radius and varying time. Since the radius of a single shell is set by the time ($R = vt$), that combination is not possible with a single shell. Rather, constant radius with varying time is a central engine: the central source provides the duration of the event through the multiple releases of energy over a time commensurate with typical burst durations. We conclude that the observations strongly argue

that a single shell is not responsible for the gamma-ray phase. Rather, a central engine is required to explain the duration and chaotic nature of GRBs.

Acknowledgments. This work done under the auspices of the US Department of Energy.

References

- Akerlof, C. W., et al. 1999, *Nature* 398, 400
Band, D., et al., 1993, *ApJ*, 413, 281
Dermer, C. D., & Mitman, K. E., 1999, *ApJ*, submitted, astro-ph/9809411
Fenimore, E. E., 1999, *ApJ*, 518, in press, astro-ph/9712331
Fenimore, E. E., Madras, C. D., & Nayakshin, S., 1996, *ApJ* 473, 998, astro-ph/9607163
Fenimore, E. E., Ramirez-Ruiz, E., & Wu, Bobing, 1999a, *ApJL*, 518, in press, astro-ph/9902007
Fenimore, E. E., et al., 1999b, *ApJ*, 512, 683, astro-ph/9802200.
Li, H. & Fenimore, E. E., 1996, *ApJ* 469, L115
Meegan, C. A., et al. 1996, *ApJS*, 106, 65
Mészáros, P., & Rees, M. J., 1993, *ApJ*, 405, 278
Mitrofanov, I. G., Litvak, M. L., & Ushakov, D. A., 1997, *ApJ* 490, 509
Norris, J. P., et al., 1996, *ApJ* 459, 393
Piro, L., Matt, G., & Ricci, R., 1997, *A&A Supplement Series* 126, 524
Ramirez-Ruiz, E., & Fenimore, E. E., 1999, *A&A Supplement, Proc. Of the Rome Conf. Gamma-Ray Bursts in the Afterglow Era*, in press, astro-ph/9812426
Rees, M. J., & Mészáros, P., 1994, *ApJ*, 430, L93
Sari, R., & Piran, T., 1997, *ApJ*, 485, 270
Sari, R., & Piran, T., 1999a, *ApJ*, 502, in press, astro-ph/9901338
Sari, R., & Piran, T., 1999b, *ApJL*, 517 L109, astro-ph/9902009